JACS
JOURNAL OF THE AMERICAN CHEMICAL SOCIETY
Article
pubs.acs.org/JACS

Mechanism of the Formation of Carboxylate from Alcohols and Water Catalyzed by a Bipyridine-Based Ruthenium Complex: A Computational Study

Haixia Li and Michael B. Hall*

Department of Chemistry, Texas A&M University, College Station, Texas 77843-3255, United States

Supporting Information

ABSTRACT: The catalytic mechanism for oxidizing alcohols to carboxylate in basic aqueous solution by the bipyridine-based ruthenium complex **2** (BIPY-PNN)Ru(H)(Cl)(CO) (*Nat. Chem.* **2013**, *5*, 122) is investigated by density functional theory (DFT) with the ωB97X-D functional. Using water as the oxygen donor with liberation of dihydrogen represents a safe and clean process for such oxidations. Under NaOH, the active catalyst is **3** (BIPY-PNN)Ru(H)(CO). Four steps are involved: dehydrogenation of alcohol to aldehyde (Step 1); coupling of aldehyde and water to form the gem-diol (Step 2); dehydrogenation of gem-diol to carboxylic acid (Step 3); and deprotonation of carboxylic acid to carboxylate anion under base (Step 4). The dehydrogenations of alcohol (Step 1) and gem-diol (Step 3) prefer the double hydrogen transfer mechanism to the β-H elimination mechanism. The coupling of aldehyde and water (Step 2) proceeds through cleavage of water by catalyst **3** followed by concerted hydroxyl and hydrogen transfer to the aldehyde. The formation of the carboxylate anion occurs via direct deprotonation of the carboxylic acid under base (Step 4), while in the absence of base a stable carboxylic acid-addition complex **6** was formed. Added base was found to play important roles in the generation of catalyst **3** from both the stable carboxylic acid-addition complex **6** and its chloride precursor complex **2**. The chemoselectivity for the formation of carboxylic acid rather than ester is ascribed to the favorable cleavage of water and the subsequent generation of the stable carboxylate anion that leads to carboxylic acid upon acidification.

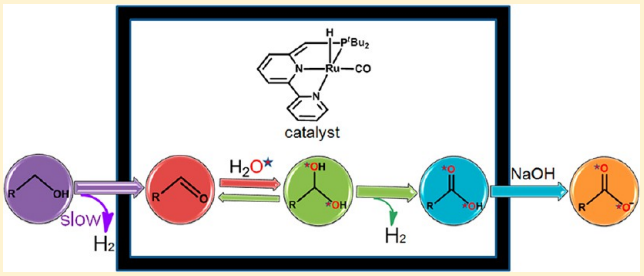

1. INTRODUCTION

Catalytic oxidation of alcohols to produce carboxylic acids represents an important process in the synthesis of bulk and fine chemicals. Most of the traditional methods for this transformation require expensive and nonatom-conserving toxic oxidizing agents (e.g., iodate, chlorite, or chromium agents), generating abundant waste.[1] Recently, cleaner and more efficient oxidations that use dioxygen or hydrogen peroxide as agents have made some progress.[2] However, the highly pressurized dioxygen that is required for efficient transformations is problematic, and additional sacrificial hydrogen acceptors such as ketone and dimethylsulfoxide (DMSO) are often needed, impeding further development in this area.[3] Therefore, greener and more economical methods for the synthesis of carboxylic acids and their derivatives from alcohols are in demand. An attractive approach toward this transformation is to use water as the oxygen donor with liberation of hydrogen gas. Such a conversion has been reported with heterogeneous catalysts at high temperature (320 °C);[4a] a related reaction was only marginally catalytic under nitrogen at 160 °C.[4b] In the first report of this homogeneous catalysis using water and producing H_2, Milstein and co-workers show that the reaction proceeds with high turnovers and high yields under mild conditions.[5]

Previously, Milstein and co-workers designed a series of pincer ruthenium complexes that exhibit high catalytic activity for σ-bond (X−H, X = H, C, O, and N) cleavage and new bond (X−C, X = O and N) formation.[6] For example, the ruthenium complexes in Figure 1 are reported to catalyze the dehydrogenative coupling reactions of alcohols with themselves or amines to produce esters and amides, respectively.[7] They are also used to perform hydrogenation of carbonates and carbamates, which provides an indirect way to transform CO_2 to methanol, representing an important C_1 conversion.[8] Furthermore, complex **1** was reported to split H_2O into O_2 and H_2, an important development in renewable energy research.[9] Recently, the same group has developed another remarkable utilization of the ruthenium complexes, where complexes **2** and **3** were

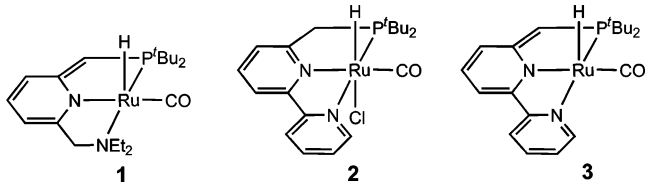

Figure 1. Ruthenium complexes designed by Milstein and co-workers.

Received: October 18, 2013
Published: December 13, 2013

   dx.doi.org/10.1021/ja410541v | *J. Am. Chem. Soc.* 2014, 136, 383−395

Scheme 1. Hydrogen Activation under the Catalyst Model Cat^{model}

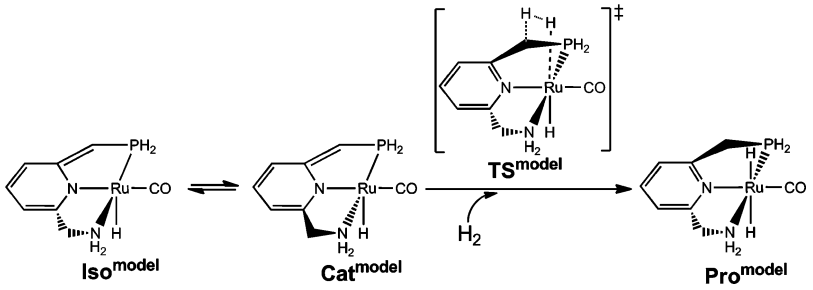

reported to catalyze the conversion of alcohols and water to carboxylic acid salts in basic solution.[5] The subsequent acid extraction produces the carboxylic acids. The only byproduct of this reaction is hydrogen gas. Remarkably, water acts as both the oxygen donor and reaction medium in this transformation, and no additional hydrogen acceptors are needed. In contrast with the previous study of the synthesis of esters from alcohols catalyzed by complex **1**,[7a] no trace of ester was observed in this reaction. Furthermore, Brønsted basic media (NaOH) is required to reform the catalyst.[5]

The importance of this reaction and its remarkable characteristics inspired us to conduct computational studies on the catalytic mechanism, because the understanding of catalytic reaction mechanisms can help researchers to improve current and develop new catalysts and reactions. Although a mechanism was proposed and DFT calculations were performed on a few intermediates, transition states and alternative pathways were not investigated. Herein, we investigated this reaction in detail, examined alternative mechanistic steps, and collected the most favorable pathways into a single mechanism. The catalytic role of related ruthenium complexes was previously studied with DFT calculations by several groups.[10−16] The reactivity of the pincer complexes is found to originate from their novel metal−ligand cooperative effect that is based on the ligand's noninnocence, which allows transformation of the central pyridine ring to change its aromaticity while changing the bonding to the metal.

2. COMPUTATIONAL DETAILS

Calculations were conducted by using the Gaussian 09 programs[17] with ωB97X-D functional.[18] This functional contains both exchange and dispersion corrections that play important roles in correctly describing both bond changes and weak interactions. The relative electronic energies of this functional are calibrated against the CCSD and CCSD(T) results. The caliberation was conducted by calculating the hydrogen activation under the catalyst model **Cat^{model}** (Scheme 1). Geometries were optimized in the gas phase with the ωB97X-D functional at the BS1 level, all-electron 6-31G(d,p) for nonmetal atoms[19] and SDD for Ru.[20] The key word "int=ultrafine" with a pruned (99,590) grid was used to optimize large molecules with many soft modes such as methyl rotations, making such optimizations more reliable. Using these geometries, single point calculations were conducted at the BS2 level, all-electron 6-31++G(d,p) for nonmetal atoms[21] and SDD for Ru. Using the Molpro program,[22] single point calculations with CCSD and CCSD(T) functionals were performed at the BS3 level, all-electron 6-311++G(d,p) for nonmetal atoms and aug-cc-pVTZ-PP for Ru. For this model reaction, which is representative of many of key steps in the mechanism, the ωB97X-D functional produces results very close to those from CCSD and CCSD(T) (Table 1).

Geometries of all intermediates and transition states in the mechanistic study were also optimized in the gas phase at the BS1 level with the key word "int=ultrafine". Water (solvent) is considered to play important roles in the deprotonation processes under OH^- (Figures 11 and 13);[23] thus, the same functional and basis set but in water (ε=78.3553) with the SMD solvent model[24] was used to optimize the involved geometries. Harmonic vibrational frequencies were calculated to identify intermediates with no imaginary frequency and transition states with only one imaginary frequency.[25] The harmonic frequencies obtained after geometry optimizations were used for the thermal and entropic corrections for enthalpies and free energies at 298 K and 1 atm. On the basis of the optimized geometries in gas phase or water, the energetic results were further refined by single-point calculations with the SMD solvent model (in water) by using the same functional ωB97X-D, but with the higher-level basis set, BS2. An adjustment for 1 atm to 1 M standard-state concentration of RT ln(24.5), that is, 1.9 kcal/mol, was used for all the species in aqueous solution except for water itself, for which the adjustment for 1 atm to 55.6 M standard-state concentration of RT ln(55.6), 4.3 kcal/mol, was employed (see the Supporting Information).[26] Solvation free energies were added to the free energies with the above adjustments for the standard-state concentration and the enthalpies at the higher-level basis set BS2 to produce the $\Delta G[\Delta H]$ reported here. Some species in this study were found to optimize in more than one geometry, and the geometry used here is the most favorable one. The JIMP2 molecular visualizing and manipulating program was employed to draw all the 3D molecular structures involved in this study.[27] The Ru−CO bond order is greater than 1.0, and the software shows the bond as a double bond.

Table 1. Energy Results for the Hydrogen Activation with Different Functionals[a]

functionals	Iso^{model}	TS^{model}	Pro^{model}
ωB97X-D/BS2//ωB97X-D/BS1	0.1	10.9	−20.5
CCSD/BS3//ωB97X-D/BS1	0.1	12.5	−20.9
CCSD(T)/BS3//ωB97X-D/BS1	0.1	9.6	−21.7

[a]Values in the table are electronic energies in kcal/mol relative to the separate **Cat^{model}** and H_2.

3. RESULTS AND DISCUSSION

In a catalytic reaction, the electronic and geometric structures of both catalyst and substrates have significant influences on the catalytic reactivity. Thus, it is preferable to use the active catalyst and substrates as are done here rather than truncated models in the calculations. Various alphatic and aromatic alcohol substrates were used in the experiment with the reaction yields varying from 61% to 91%.[5] Among them, eq 1 was chosen as a representative

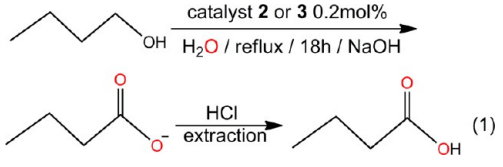

reaction in this study, because it has a high yield (80%) and the substrate *n*-butyl alcohol is relatively small, thereby reducing the computational cost.

dx.doi.org/10.1021/ja410541v | J. Am. Chem. Soc. 2014, 136, 383−395

Scheme 2. Several Species Involved in the Catalysis

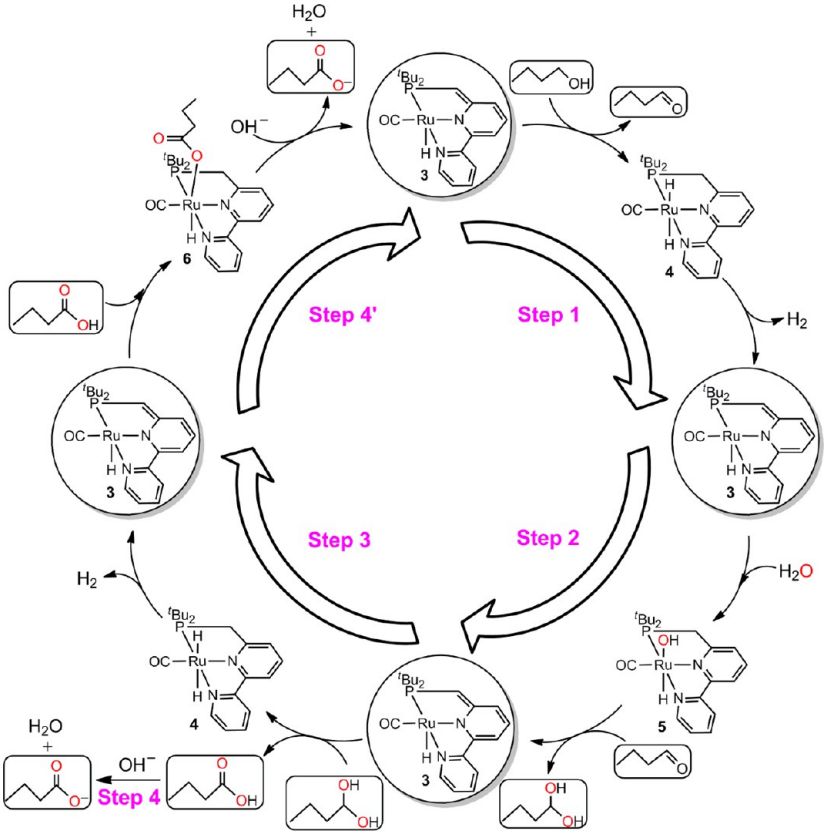

Figure 2. Overall four-step mechanism for the formation of the carboxylate anion from alcohol and water.

On the basis of their experimental work, Milstein and co-workers proposed a mechanism that involves several species generated during the four steps in Scheme 2: alcohol dehydrogenates to generate aldehyde (Step 1); aldehyde couples with water to form gem-diol (Step 2); gem-diol dehydrogenates to give carboxylic acid (Step 3); and carboxylic acid deprotonates to afford carboxylate anion under base (Step 4). The species, aldehyde, gem-diol, and carboxylic acid, were also proposed as short-lived intermediates for other similar reactions.[3a,28] However, in examining some obvious transition states for these steps, high barriers were found. Thus, we undertook a computational examination of the reaction mechanism to find lower-barrier steps. In addition, we used these steps to explain the labeling experimental results, where both oxygen atoms of the carboxylate anion originate from water.

The details of the four-step mechanism are described in section 3.1 by presenting key transition states and intermediates. Inspired by the mechanism for the generation of catalyst **3** from the carboxylic acid-addition complex under base, the mechanism for the formation of catalyst **3** from its precursor chloride complex **2** under base is explained in section 3.2. The chemoselectivity for the formation of carboxylic acid over ester is discussed in section 3.3.

3.1. Four-Step Mechanism for the Generation of Carboxylate Anion from Alcohol. The proposed four-step mechanism (Scheme 2) is somewhat similar to the mechanism for the formation of amides from primary alcohols and amines catalyzed by complex **1**, which produces hemiaminal as an intermediate by coupling amine with aldehyde.[16a] However, the details of the two mechanisms are different.

Figure 2 shows the overall four-step mechanism for the formation of the carboxylate anion from alcohol and water with the active catalyst **3**. The catalyst first dehydrogenates alcohol to aldehyde and forms the *trans*-dihydride ruthenium complex **4**, which releases hydrogen to regenerate catalyst **3** (Step 1). The dehydrogenation of alcohol to aldehyde is always considered as the first step of coupling reactions that use alcohol as a substrate.[29] In Step 2, water adds to catalyst **3** to form complex **5**, followed by the concerted transfer of the hydroxyl group and hydrogen atom from complex **5** to aldehyde, leading to gem-diol with regeneration of catalyst **3**. It should be noted that the gem-diol with two labeled oxygen atoms might seem to be inconsistent with the product formed directly from complex **5** and aldehyde where there is only one labeled oxygen atom. The apparent discrepancy is due to exchange with the high concentration of labeled water, and the details will be addressed in section 3.1.3. Subsequently, the gem-diol dehydrogenates to form carboxylic acid and the *trans*-dihydride ruthenium complex **4**, which then releases hydrogen to reform catalyst **3** (Step 3). This step is similar to Step 1. In Step 4, the carboxylic acid deprotonates to carboxylate anion directly under base. In the absence of base, the carboxylic acid adds to catalyst **3** to give the

dx.doi.org/10.1021/ja410541v | J. Am. Chem. Soc. 2014, 136, 383−395

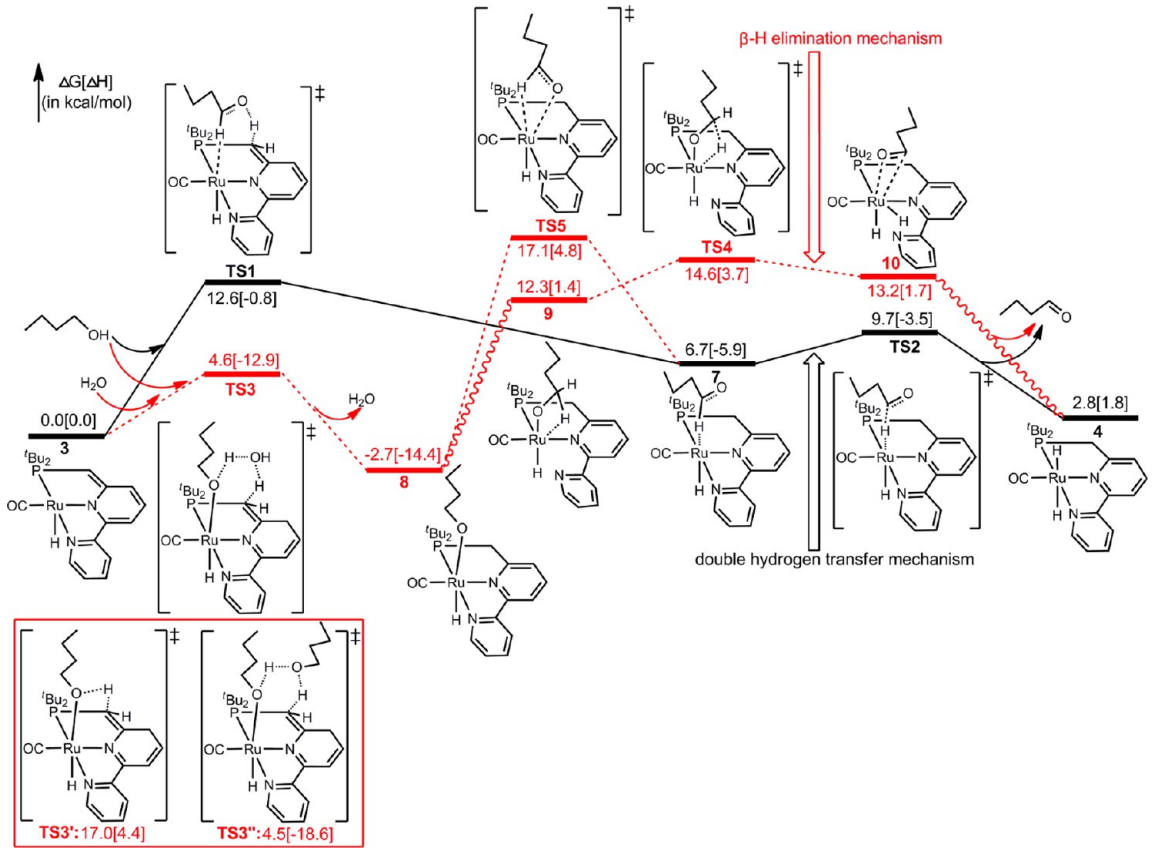

Figure 3. Energy profiles for the dehydrogenation of alcohol via the double hydrogen transfer mechanism (solid line) or the β-H elimination mechanism (broken line).

ruthenium complex **6**, followed by deprotonation to form the carboxylate anion with regeneration of catalyst **3** when base is added (Step 4′). The computed results for these steps are discussed in the following subsections, respectively.

3.1.1. Dehydrogenation of Alcohol to Aldehyde. Figure 3 shows the energy profiles for the dehydrogenation of alcohol via two mechanisms: the double hydrogen transfer mechanism (solid line) and the β-H elimination mechanism (broken line). Optimized geometries of selected intermediates and transition states are shown in Figure 4.

In the double hydrogen transfer mechanism (solid line in Figure 3), the proton on O first transfers to the C═C bond (on the $-P(^tBu)_2$ ligand) via transition state **TS1**, leading to an intermediate, **7**. Subsequently, the hydride transfers to the ruthenium center via transition state **TS2**, generating the *trans*-dihydride complex **4** with liberation of the aldehyde. Relative to the separate catalyst **3** and *n*-butyl alcohol, the barriers for transition states **TS1** and **TS2** are 12.6[−0.8] and 9.7[−3.5] kcal/mol, respectively. In this path, proton transfer is the rate-determining process, and then intermediate **7** rapidly undergoes hydride transfer to generate the aldehyde. The *trans*-dihydride ruthenium complex **4** and aldehyde are 2.8[1.8] kcal/mol above the separate catalyst **3** and *n*-butyl alcohol. In the optimized geometry of catalyst **3** (Figure 4), the C═C bond on the $-P(^tBu)_2$ ligand has a bond length of 1.38 Å and the central pyridine ligand has an alternating C−C and C═C bond, showing the characteristics of dearomatization. In contrast, complex **4** shows the characteristics of aromatization with the C−C bond on the $-P(^tBu)_2$ ligand at 1.50 Å, and the central pyridine ligand with equal C−C bond. Thus, the transformation between dearomatization and aromatization plays an important role in this process. In the proton transfer transition state **TS1**, the breaking O−H bond is 0.44 Å longer than that in free alcohol. The agostic C−H···Ru bond interaction stabilizes intermediate **7**, which shows a quite long C−H bond of 1.32 Å. In the hydride transfer transition state **TS2**, the breaking C−H bond is only 0.22 Å longer than that in intermediate **7**. Thus, **TS2** is an early transition state, consistent with the rapid hydride transfer process.

The β-H elimination mechanism (broken line in Figure 3) starts with the addition of alcohol to catalyst **3** over transition state **TS3** involving a water molecule as a proton shuttle. Relative to the separate catalyst **3** and *n*-butyl alcohol, the barrier for the transition state **TS3** is 4.6[−12.9] kcal/mol, which is lower than that (17.0[4.4] kcal/mol) for the direct O−H bond cleavage transition state **TS3′**, implying that water as a proton shuttle facilitates this process. Although a second alcohol could act as a proton shuttle to slightly lower the barrier to 4.5[−18.6] kcal/mol (**TS3″**), in the experimental system, hydrogen-bond interactions between the solvent water and the mediator water may further stabilize **TS3**.[30] In contrast, the alcohol-mediated transition state **TS3″** would not have such strong hydrogen-bond interactions. Thus, water-catalyzed pathway should dominate under these conditions. In the following discussions, only the water-catalyzed pathway is reported, and the alcohol-catalyzed pathway is considered for comparison purposes if necessary. After **TS3**, the ruthenium alkoxide complex **8** is more stable by 2.7[14.4] kcal/mol than the separate catalyst **3** and alcohol. Optimized geometries in Figure 4 are consistent with the above discussions. In **TS3**, water functions as a proton shuttle with the

dx.doi.org/10.1021/ja410541v | J. Am. Chem. Soc. 2014, 136, 383−395

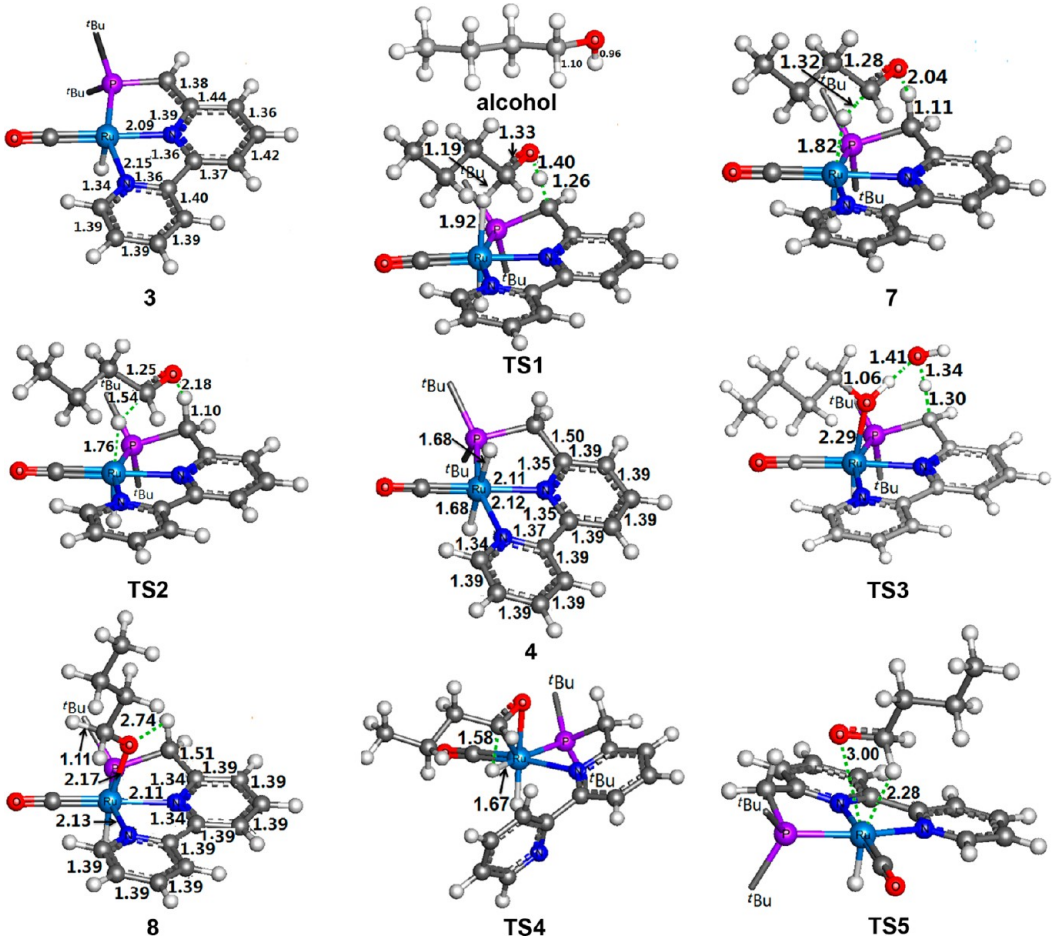

Figure 4. Optimized geometries of selected intermediates and transition states involved in Figure 3. Key bond lengths are given in angstroms, and *tert*-butyl groups are omitted for clarity. Additional optimized geometries are available in the Supporting Information.

breaking and forming O−H bond lengths at 1.34 and 1.41 Å, respectively. In complex **8**, the central pyridine ring becomes aromatic and there is a hydrogen-bond interaction between the two atoms of the broken O−H bond (see Figure 4).

To undergo β-H elimination, an unsaturated 16e$^-$ complex is required to accept the eliminating β-C−H bond. Because Ru^{II}−P coordination is stronger than Ru^{II}−N coordination, as shown in a previous study,[16b] the terminal pyridine ligand in complex **8** dissociates to generate a vacant site on the ruthenium atom. The transition state for this process is not shown in Figure 3, but its barrier should be low, because the previous study of complex **1** shows that its $-NEt_2$ ligand dissociates easily.[16a] Complex **9** with the terminal pyridine ligand dissociated is less stable by 15.0[15.8] kcal/mol than complex **8**. The barrier for the subsequent β-H elimination transition state **TS4** is 17.3[18.1] kcal/mol relative to complex **8**, and is 14.6[3.7] kcal/mol relative to the separate catalyst **3** and *n*-butyl alcohol. In the optimized geometry of **TS4** (Figure 4), the eliminating C−H bond is elongated by 0.47 Å from that in complex **8**. After **TS4**, complex **10** then proceeds via the dissociation of aldehyde, hydride movement, and reassociation of the terminal pyridine ligand to generate complex **4**; these processes are not shown in Figure 3. Overall, the barrier for the β-H elimination transition state **TS4** is higher by 2.0[4.5] kcal/mol than that for the rate-determining transition state **TS1** in the double hydrogen transfer mechanism. Calculations of **TS1** and **TS4** by using other functionals, M06, TPSS, and LC-ωPBE, maintain the trend (see the Supporting Information). Therefore, the β-H elimination mechanism is less favorable than the double hydrogen transfer mechanism. **TS4** in the β-H elimination mechanism is unfavorable because it is a compact inner-sphere transition state where the alcohol needs to come into the ruthenium center, causing steric repulsions. In contrast, **TS1** and **TS2** in the double hydrogen transfer mechanism have more outer-sphere character where the alcohol's oxygen atom is not bound to the ruthenium center.[16a,b] Furthermore, the dissociation of the pyridine ligand destabilizes **TS4**, disfavoring the β-H elimination mechanism.

An alternative mechanism with a crossing between the two pathways via transition state **TS5** was considered. The optimized geometry of the four-member-ring transition state **TS5** corresponds to simultaneously dissociating the alkoxide group and forming an agostic β-C−H···Ru bond interaction, thus connecting complex **7** in the double hydrogen transfer pathway and complex **8** in the β-H elimination pathway. This mechanism avoids undergoing the unfavorable β-H elimination transition state **TS4**. However, **TS5** is still higher by 4.5[5.6] kcal/mol than **TS1**. Therefore, this alternative mechanism is also less favorable than the double hydrogen transfer mechanism.

The conclusion that the dehydrogenation of alcohol prefers the double hydrogen transfer mechanism in this system is consistent with those in the previous ruthenium complex **1** and its analogues.[16a,b] In contrast, the previous experimental study observed the ruthenium alkoxide complex corresponding to complex **8**,[31] and as Figure 3 shows the calculations agree that

dx.doi.org/10.1021/ja410541v | J. Am. Chem. Soc. 2014, 136, 383−395

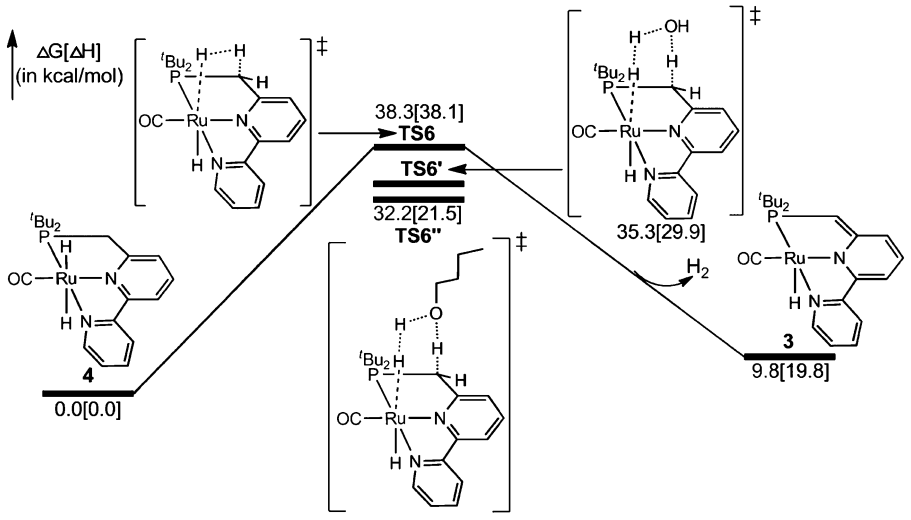

Figure 5. Energy profiles for hydrogen release from the *trans*-dihydride ruthenium complex **4**.

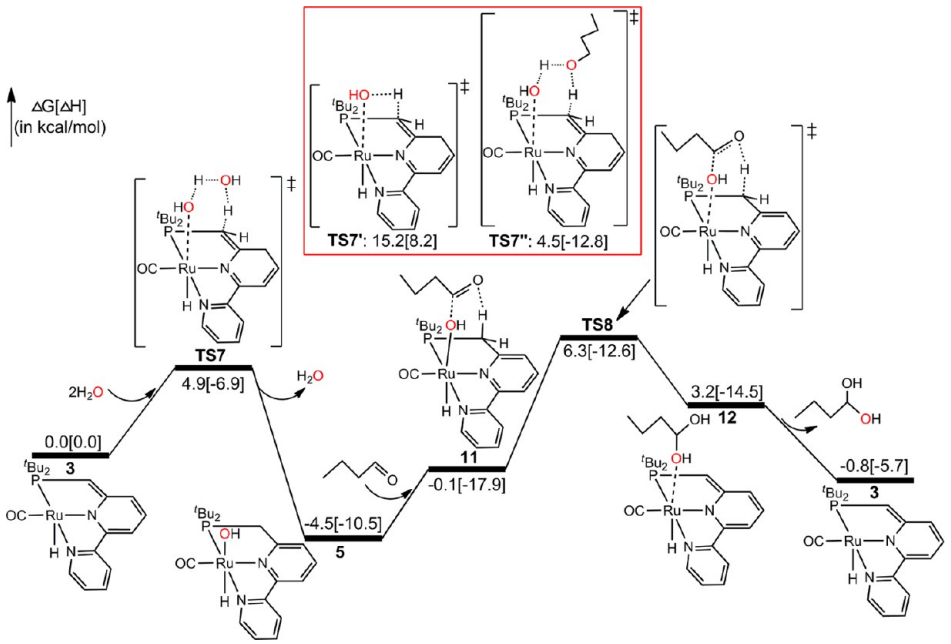

Figure 6. Energy profile for the coupling of aldehyde and water to form the gem-diol.

complex **8** is stable on the energy surface. However, the observation of this ruthenium alkoxide complex does not violate the conclusion that the double hydrogen transfer mechanism is favored for the dehydrogenation of the alcohol. This can be explained by using the energy profiles in Figure 3. When the ruthenium alkoxide complex **8** is formed, it can go forward over the β-H elimination transition state **TS4** to form aldehyde, or go backward over transition state **TS3** to regenerate catalyst **3** and alcohol. The barrier for the forward transition state **TS4** is higher by 10.0[16.6] kcal/mol than that for the backward transition state **TS3**. In addition, complex **8** is not very stable, only −2.7[−14.4] kcal/mol relative to the separate catalyst **3** and alcohol. Therefore, complex **8** exists in high concentration, but regenerates catalyst **3** and alcohol, which then proceed via the double hydrogen transfer mechanism to form aldehyde. Furthermore, Milstein and co-workers demonstrated in their experimental work that alcohol addition is reversible and indicated that the β-H elimination mechanism is unlikely.[31]

After release of the aldehyde, the *trans*-dihydride ruthenium complex **4** needs to release hydrogen to regenerate catalyst **3**. Figure 5 shows three pathways: direct hydrogen release over transition state **TS6** and water- or alcohol-catalyzed hydrogen release over transition states **TS6′** and **TS6″**, respectively. The barriers for **TS6**, **TS6′**, and **TS6″** are 38.3[38.1], 35.3[29.9], and 32.2[21.5] kcal/mol, respectively. The hydrogen release in this step is calculated to be the rate-determining process in comparison with the other steps. Although the water-catalyzed hydrogen release transition state **TS6′** is somewhat less favorable than the alcohol-catalyzed transition state **TS6″**, hydrogen-bond interactions between the solvent water and the mediator water likely drives the step over **TS6′**. An alternative hydrogen release pathway from complex **8** by eliminating the proton on the $-P(^tBu)_2$ ligand and the hydride on the ruthenium atom was considered.[5] The barriers are 46.9[45.0] and 43.3[37.3] kcal/mol for the direct and water-catalyzed pathways, respectively. Therefore, the hydrogen release from complex **8** is computed to

dx.doi.org/10.1021/ja410541v | J. Am. Chem. Soc. 2014, 136, 383−395

be less favorable than the hydrogen release from complex **4**. Unfavorable hydrogen release pathways are deposited in the Supporting Information.

3.1.2. Coupling of Aldehyde and Water to Form the Gem-diol. Figure 6 shows the energy profile for the coupling of aldehyde and water to form gem-diol. Optimized geometries of transition states and selected intermediates are drawn in Figure 7.

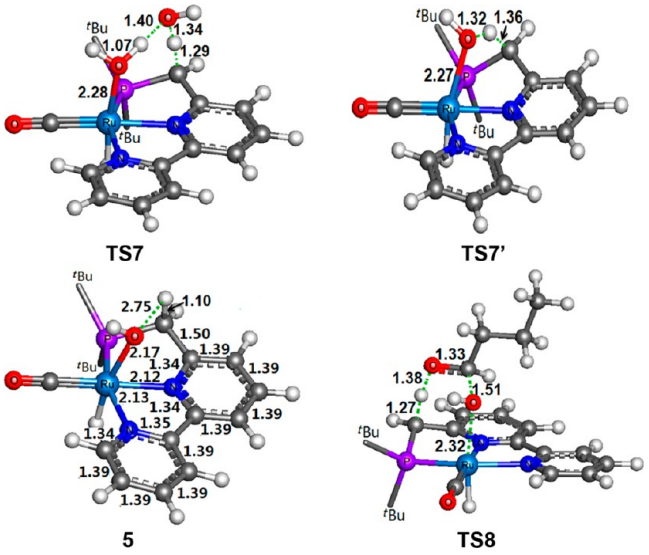

Figure 7. Optimized geometries of transition states and selected intermediates involved in Figure 6. Key bond lengths are given in angstroms, and *tert*-butyl groups are omitted for clarity. More optimized geometries are in the Supporting Information.

First, water adds to catalyst **3** over transition state **TS7** with another water molecule as a catalyst for a proton shuttle, generating complex **5**. Although previous studies for the water splitting by the ruthenium complex **1** proposed a direct mechanism, with no additional water as a proton shuttle (as **TS7′**),[11,14,15] the water-catalyzed transition state **TS7** is 10.3[15.1] kcal/mol more favorable than that for the direct water cleavage transition state **TS7′**. **TS7′** is clearly more strained than **TS7** (Figure 7); the breaking O−H bond of water bonding to the Ru atom is longer by 0.25 Å and the five-membered ring on the ligand's $-P(^tBu)_2$ side is more twisted. Thus, water-catalyzed transition state **TS7** avoids this significant strain energy. Consistent with the experimental results, water adds to catalyst **3** reversibly, and the water splitting product **5** is −4.5[−10.5] kcal/mol relative to the separate catalyst **3** and water. The central pyridine ring is again aromatic in the optimized geometry of complex **5**.

Subsequently, aldehyde attacks complex **5**, and then the −OH group and H atom transfer simultaneously from complex **5** to the aldehyde over a concerted transition state **TS8** that was confirmed by IRC analyses. In the optimized geometry of **TS8** (Figure 7), the breaking Ru−OH and C−H bond are elongated by 0.15 and 0.17 Å, respectively, from those in complex **5**, a geometry consistent with a concerted transition state. Complex **12** is 4.0[−8.8] kcal/mol relative to the separate gem-diol and catalyst **3**, so it will readily release the gem-diol. Alternative mechanisms for producing the gem-diol, including the direct pathway without catalyst **3** and the pathway over a three-molecule transition state involving catalyst **3**, water, and alcohol, are calculated to be unfavorable (see the Supporting Information).

3.1.3. Dehydrogenation of Gem-diol to Carboxylic Acid. Figure 8 shows the energy profile for the dehydrogenation of the

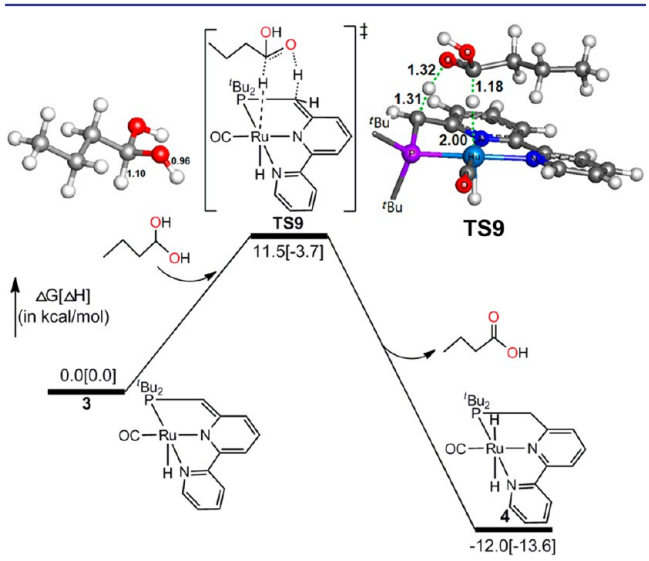

Figure 8. Energy profile for the dehydrogenation of the gem-diol via the double hydrogen transfer mechanism. Key bond lengths are given in angstroms, and *tert*-butyl groups are omitted for clarity.

gem-diol via the double hydrogen transfer mechanism that is similar to the dehydrogenation of the alcohol (section 3.1.1). In contrast to the stepwise mechanism over transition states **TS1** and **TS2** for the dehydrogenation of the alcohol (Figure 3), the dehydrogenation of the gem-diol proceeds over a concerted transition state **TS9** where the proton and hydride transfer simultaneously. All optimizations of the stepwise transition-state structures, where the proton and hydride transfer separately, repeatedly converge to **TS9**. Convergence to alternative stepwise transition-state structures can only be obtained with the different arrangement of the gem-diol relative to the catalyst, but it is unfavorable (see the Supporting Information). In the optimized geometry of **TS9**, the breaking O−H bond and C−H bond are respectively elongated by 0.36 and 0.08 Å from those in the free gem-diol. Thus, **TS9** is somewhat asynchronous where the proton transfer leads, and the hydride transfer follows it, a sequence similar to that in the dehydrogenation of the alcohol. After crossing a barrier of 11.5[−3.7] kcal/mol for **TS9**, the *trans*-dihydride complex **4** and carboxylic acid are more stable than the separate reactants by 12.0[13.6] kcal/mol. Therefore, this step is favorable both kinetically and thermodynamically.

In the experiment, both oxygen atoms of the carboxylic acid were observed to come from water.[5] Since the carboxylic acid is formed from the dehydrogenation of the gem-diol (Figure 8), both oxygen atoms of the gem-diol need to come from water. However, Figure 6 shows that only one oxygen atom of the gem-diol comes from water, and the other one is from aldehyde. The energy profile from the combination of Figures 6 and 8 as shown in Figure 9 explains this apparent inconsistency. The gem-diol can either dehydrogenate to the carboxylic acid over transition state **TS9** (forward), or decompose into aldehyde and water over transition states **TS8** and **TS7** (backward). The backward process allows the aldehyde and water to exchange their oxygen atoms. Since the barrier for the forward transition state **TS9** is higher than both the backward transition states **TS8** and **TS7** by 4.4 and 5.8 kcal/mol in free energy, respectively, oxygen exchange with water, which is in high concentration, should be

dx.doi.org/10.1021/ja410541v | J. Am. Chem. Soc. 2014, 136, 383−395

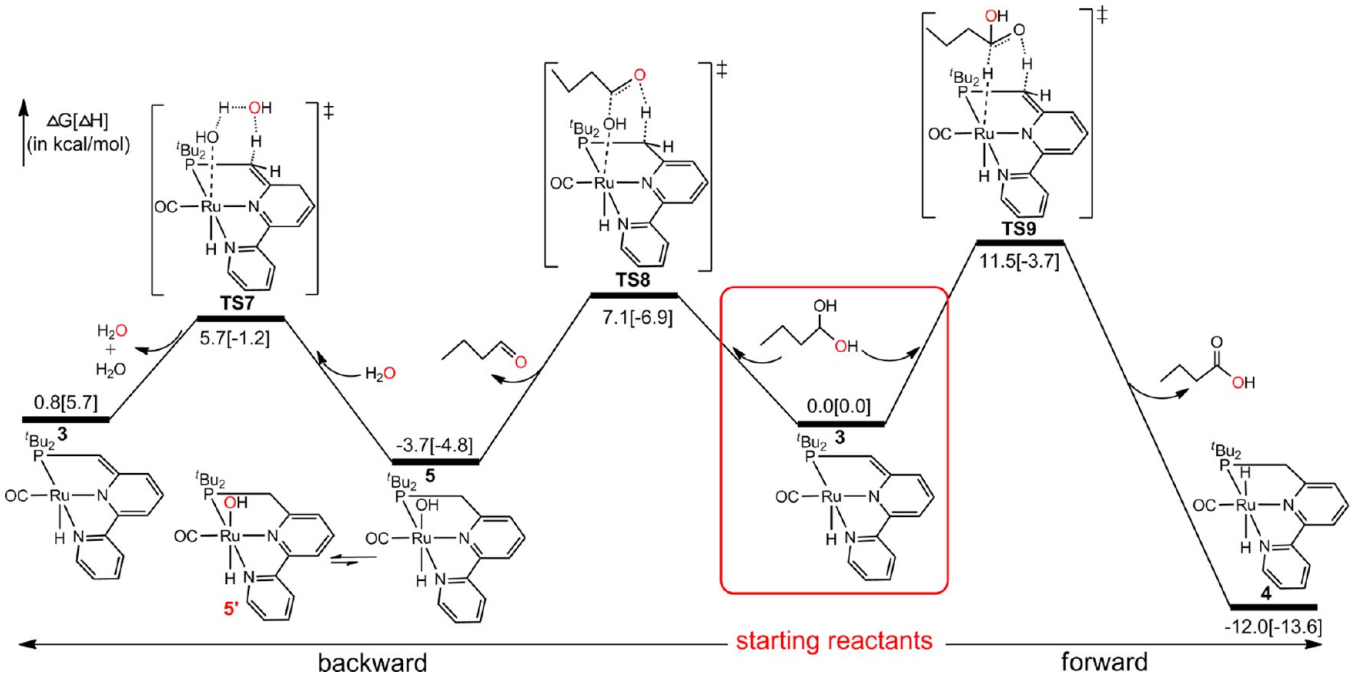

Figure 9. Energy profile for the backward and forward reactions from the gem-diol.

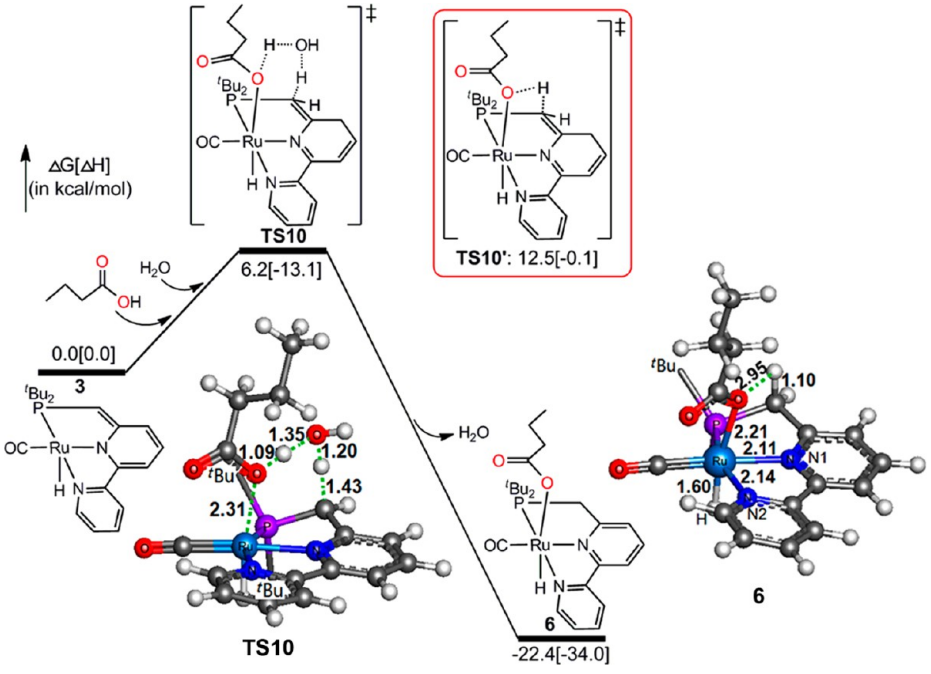

Figure 10. Energy profile for the cleavage of the carboxylic acid O−H bond by catalyst **3** to form the ruthenium complex **6**. Key bond lengths are given in angstroms, and *tert*-butyl groups are omitted for clarity. Selected bond lengths for X-ray structure of the carboxylic-acid addition complex formed between acetic acid and catalyst **3**: Ru−O, 2.200(3); Ru−H, 1.55(5); Ru−N1, 2.092(4); Ru−N2, 2.117(4).

rapid. The addition of water to the regenerated catalyst **3** from complex **5** forms an intermediate **5′**, resulting in repeated exchanges of labeled and unlabeled oxygen atoms between complex **5** and **5′**; the equilibrium favors the formation of **5′**. Therefore, both the oxygen atoms of the gem-diol finally come from water.

3.1.4. Deprotonation of Carboxylic Acid to Carboxylate Anion under Base. The carboxylic acid generated from the dehydrogenation of the gem-diol is an intermediate that then deprotonates to the carboxylate anion and water under OH^- (Step 4). The carboxylate anion and water are more stable than the carboxylic acid and OH^- by 16.6[20.0] kcal/mol. Because water plays important roles in the deprotonation,[22] a transition-state structure for the proton transferring from the carboxylic acid to OH^- was sought in water. However, the optimizations repeatedly converged to the product, carboxylate anion, and water. The geometric scans in water with the breaking carboxylic acid O−H bond as the coordinate show that the deprotonation has no electronic energy barrier.

dx.doi.org/10.1021/ja410541v | *J. Am. Chem. Soc.* 2014, 136, 383−395

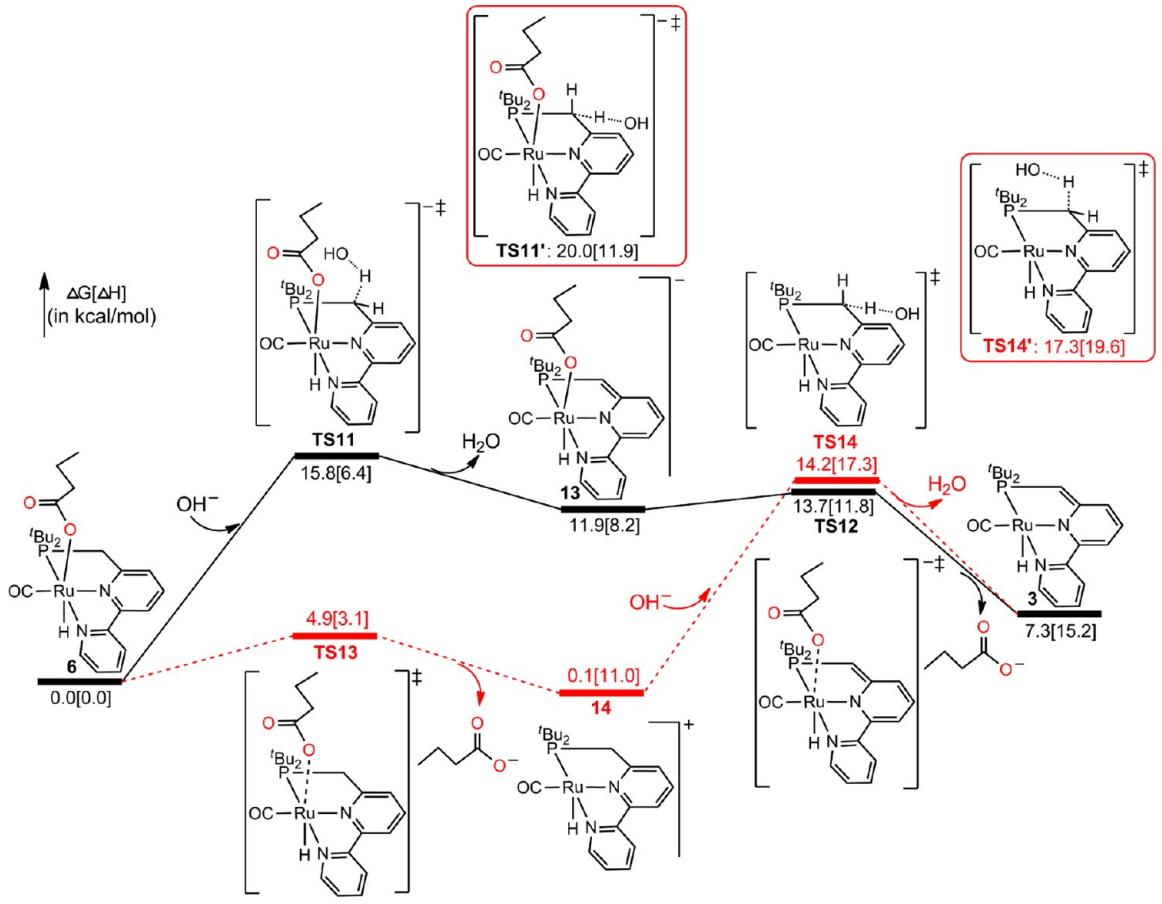

Figure 11. Energy profiles for the formation of the carboxylate anion under base via two pathways shown in solid and broken lines. Optimizations are conducted in water by using the SMD solvent model.

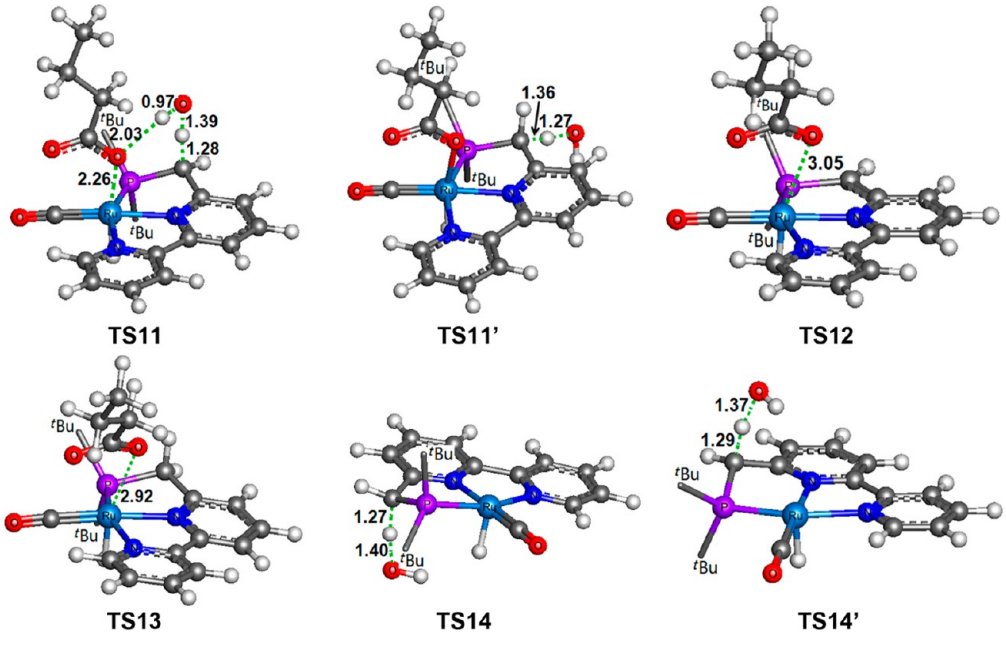

Figure 12. Optimized geometries of transition states involved in Figure 11. Key bond lengths are given in angstroms, and *tert*-butyl groups are omitted for clarity. Additional optimized geometries are in the Supporting Information.

3.1.5. Formation of the Carboxylic Acid-Addition Complex without Base Followed by the Deprotonation to Carboxylate Anion When Base Is Added. In the absence of base, a carboxylic acid-addition complex **6** was formed (Step 4′ in Figure 2). Figure 10 shows the energy profile for generating complex **6** through the cleavage of the carboxylic acid O−H bond by catalyst **3**. The barrier for the water-catalyzed transition state **TS10** is lower than that for the direct transition state **TS10′** by 6.3[13.0] kcal/mol,

dx.doi.org/10.1021/ja410541v | J. Am. Chem. Soc. 2014, 136, 383−395

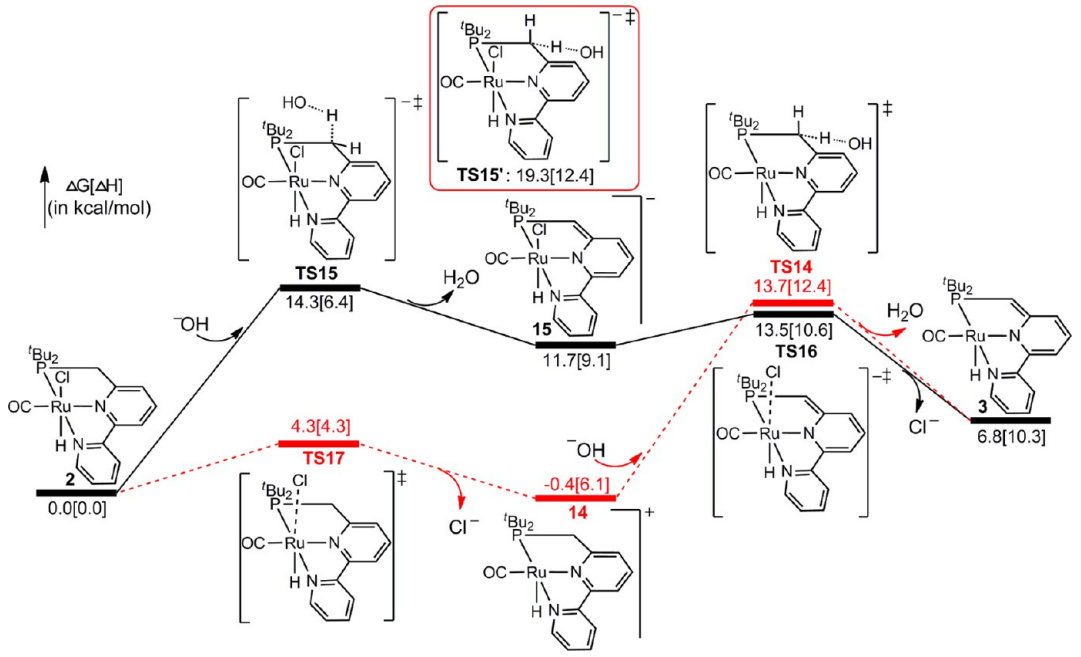

Figure 13. Energy profiles for the formation of the active catalyst **3** from its precursor ruthenium chloride complex **2** under OH^- via two pathways shown as solid and broken lines. Optimizations are conducted in water by using the SMD solvent model.

demonstrating that water again acts as a proton shuttle and facilitates this process. Complexes formed by either oxygen atom of the carboxylic acid coordinated to the ruthenium atom of catalyst **3** are unstable. Complex **6** is more stable than the separate catalyst **3** and carboxylic acid by 22.4[34.0] kcal/mol. A corresponding carboxylic acid-addition complex was observed in experiments for the reaction of water and 1-hexanol or ethanol under the catalytic conditions but without base.[5] Furthermore, most 1-hexanol and ethanol remained unreacted, because the formation of the stable complex like **6** deactivates catalyst **3**. In addition, the equilibrium between the free carboxylic acid and the carboxylic acid-addition complex results in the experimental observations of small amounts of free carboxylic acid. Optimized geometry of complex **6** is consistent with the X-ray structure of the carboxylic acid-addition complex formed between acetic acid and catalyst **3**.

The carboxylic acid-addition complex **6** deactivates catalyst **3**. Therefore, Brønsted base NaOH is required in the experiment to reform catalyst **3** by deprotonating complex **6**. Structures involved in this process were optimized in water, because water plays important roles in deprotonation.[22] The process involves two closely related pathways as shown in Figure 11. Optimized geometries of transition states are shown in Figure 12. In the solid-line pathway, complex **6** deprotonates first over transition state **TS11**. **TS11** is lower by 4.2[5.5] kcal/mol than transition state **TS11′** where OH^- withdraws the other hydrogen atom. The optimized geometry in Figure 12 shows a hydrogen-bond interaction with a length of 2.03 Å between OH^- and the carboxylate group, which stabilizes **TS11**; no such hydrogen-bond interaction exists in **TS11′**. Furthermore, the breaking C−H bond in **TS11′** is longer by 0.08 Å than that in **TS11**, so **TS11′** is more product-like than **TS11**. The unstable anionic complex **13** dissociates the carboxylate anion through **TS12** with a barrier of only 1.8[3.6] kcal/mol. Although the carboxylate anion and catalyst **3** are 7.3[15.2] kcal/mol higher than the separate OH^- and complex **6**, the excess OH^- drives the reaction to the carboxylate anion.

In the broken-line pathway, the carboxylate anion first dissociates easily from complex **6** through transition state **TS13** with a barrier of 4.9[3.1] kcal/mol. In the optimized geometry of **TS13** in Figure 12, the breaking Ru−O bond is longer by 0.71 Å than that in complex **6**. In the deprotonation process by OH^-, there are two transition states: **TS14** and **TS14′** where OH^- attacks the ligand from the bottom side and upper side, respectively. **TS14** is lower than **TS14′** by 3.1[2.3] kcal/mol, the C−H bond in **TS14** is less stretched than that in **TS14′** by 0.02 Å; consistently, the lower transtion states are earlier.

When comparing the two pathways, the barrier for the rate-determining transition state **TS14** in the broken-line pathway is more favorable, but the alternative pathway through **TS11** is closely competitive. In the experiment, the reaction with non-Brønsted base NBu_3 gave results similar to those with no base. This mechanistic study shows that the Brønsted base NaOH is needed, because the non-Brønsted base NBu_3 is not strong enough to deprotonate the ligand. Therefore, NBu_3 cannot affect the regeneration of catalyst **3** from the carboxylic acid-addition complex **6**.

3.2. Formation of the Active Catalyst 3 from Its Precursor Complex 2. The above mechanistic studies of the catalytic role of base inspired us to investigate the mechanism of the formation of the active catalyst **3** from its precursor ruthenium chloride complex **2** under base. Structures involved in this process were also optimized in water. Figure 13 shows energy profiles for the two pathways that are similar to those in Figure 11. Optimized geometries for transition states are shown in Figure 14. In the solid-line pathway, OH^- first attacks complex **2** and withdraws the proton from the ligand over transition state **TS15**. **TS15** is lower by 5.0[6.0] kcal/mol than transition state **TS15′** where OH^- withdraws the "bottom" proton of the ligand. Consistent with this energy difference, the breaking C−H bond in **TS15** is less stretched than that in **TS15′** by 0.09 Å, and the Cl···H interaction with length of 2.47 Å further stabilizes **TS15**. Intermediate **15** is formed next and is less stable by 11.7[9.1] kcal/mol than the separate complex **2** and OH^-. The next barrier

dx.doi.org/10.1021/ja410541v | J. Am. Chem. Soc. 2014, 136, 383−395

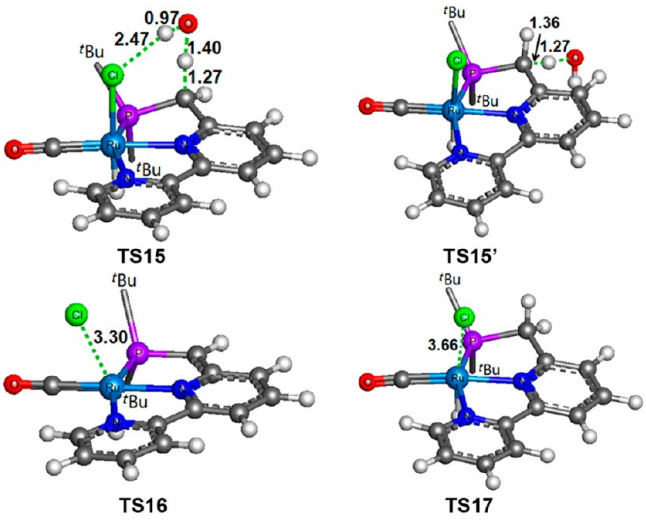

Figure 14. Optimized geometries of transition states involved in Figure 13. Key bond lengths are given in angstroms, and *tert*-butyl groups are omitted for clarity. Additional optimized geometries are in the Supporting Information.

for **TS16** corresponding to chloride anion dissociation is low, 1.8[1.5] kcal/mol above **15**. Although the formation of catalyst **3**, Cl^-, and H_2O is unfavorable by 6.8[10.3] kcal/mol, excess OH^- and favorable reactions with catalyst **3** drive this process. In the broken-line pathway, the dissociation of chloride anion is favorable by crossing a barrier of 4.3[4.3] kcal/mol for **TS17**. The next barrier, **TS14** for the deprotonation, is 14.1[6.3] kcal/mol relative to the intermediate **14**. As in the formation of the carboxyate anion described above, these two pathways also compete with each other, because the rate-determining barrier in the solid-line pathway, 14.3[6.4] kcal/mol, is comparable with that in the broken-line pathway, 14.1[6.3] kcal/mol.

The reaction examined here occurs in water, where NaOH dissociates into Na^+ and OH^-. In contrast, similar reactions studied previously often take place in neutral solvents (e.g., toluene),[6] where NaOH does not dissociate. The Supporting Information describes our study for the formation of catalyst **3** from complex **2** under NaOH in toluene.

3.3. Explanations for the Chemoselectivity for Acid Rather Than Ester. Ester formation was not observed in the experiment, and the hydrolysis of ester to acid was also excluded.[5] However, a previous study found that ester was produced from primary alcohols catalyzed by the ruthenium complex **1**.[7a] As shown in Figure 15, ester could be formed in alternatives of Step 2 and Step 3 of the mechanism described here. In the alternative Step 2, the catalyst **3** binds alcohol to form the ruthenium alkoxide complex **8**, followed by the concerted transfer of the alkoxide group and hydrogen atom to the aldehyde, generating the hemiacetal intermediate. Then in the alternative Step 3, the hemiacetal dehydrogenates to form ester. Figure 15 compares the energy profiles for this alternative route to the ester with the route to the acid described earlier. The corresponding transition states and intermediates involved in the pathway leading to ester are marked by the superscript "e". As shown in Figure 15, although the barrier for **TS7** is slightly higher than that for **TS3** by 0.3 kcal/mol, the barriers for **TS8** and **TS9** for producing acid are lower than those for the corresponding transition states **TS8**^{e} and **TS9**^{e} for producing ester by 2.3 and 2.0 kcal/mol, respectively. The calculations are consistent with the experimental observations that the reaction will produce acid rather than ester. The chemoselectivity can be explained as follows. First, the acid intermediate formed in Step 3 further deprotonates by OH^- to generate the carboxylate anion in Step 4. The carboxylate anion and water are more stable than the separate carboxylic acid and OH^- by 16.6[20.0] kcal/mol. In contrast, there are no further transformations to stabilize the ester. However, when ester is formed, it can decompose back into alcohol. Then, alcohol and water can finally produce the carboxylate anion by following the pathway of the solid line. Therefore, the formation of the stable carboxylate anion drives the whole reaction to produce the carboxylic acid rather than ester. Second, the reaction differences for the formation of carboxylic acid or ester start from the cleavage of water or alcohol

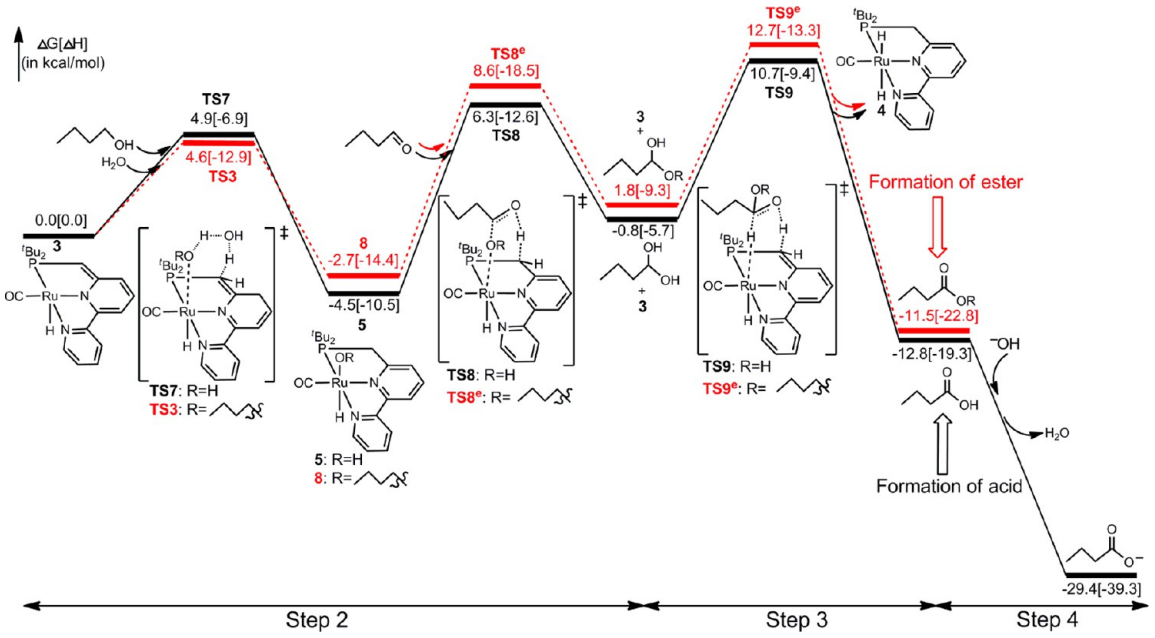

Figure 15. Comparisons of the energy profiles for the formation of acid (in solid line) and ester (the alternative steps shown in broken line), respectively.

dx.doi.org/10.1021/ja410541v | J. Am. Chem. Soc. 2014, 136, 383−395

by catalyst **3**. Although the pathway for water cleavage is less favorable than that for alcohol cleavage kinetically, it is more favorable thermodynamically, because the water cleavage product **5** is more stable than the alcohol cleavage product **8** by 1.8 kcal/mol. In addition, the hydrogen-bond interactions between the splitting water and the solvent water may favor the water cleavage pathway. Consistent with these calculations, only the water splitting product **5** was observed in a closed system without base in the experiment. Therefore, the pathway for producing acid is more favorable than that for producing ester. For further comparisons, stationary points involved in Figure 15 were recalculated with M06, TPSS, and LC-ωPBE functionals, and these methods predict that the acid pathway would even be kinetically favored over the ester pathway (see the Supporting Information).

4. CONCLUSION

In summary, DFT calculations with ωB97X-D functional were conducted to investigate the mechanism for producing a carboxylate anion from alcohol and water under a base catalyzed by the active catalyst **3**. Water is used as both solvent and oxygen donor. The studied mechanism involves four steps: dehydrogenation of alcohol to aldehyde (Step 1); coupling of aldehyde and water to form gem-diol (Step 2); dehydrogenation of gem-diol to carboxylic acid (Step 3); and deprotonation of carboxylic acid to carboxylate anion (Step 4). For the dehydrogenation steps (Step 1 and Step 3), the double hydrogen transfer mechanism is more favorable than the β-H elimination mechanism. For Step 2, the gem-diol is generated through the cleavage of water by catalyst **3**, followed by the hydroxyl group and hydrogen atom transferring to the aldehyde concertedly. The formed gem-diol can either dehydrogenate to the carboxylic acid (forward, Step 3), or decompose into aldehyde and water (backward). The backward decomposition allows the aldehyde and water to exchange their oxygen atoms, explaining the experimental observations that both oxygen atoms of the carboxylate anion come from water. The deprotonation of carboxylic acid to carboxylate anion (Step 4) occurs directly under base. In the absence of base, a stable carboxylic acid-addition complex **6** is formed, followed by the deprotonation to produce carboxylate anion when base is added. There are two competing pathways for the deprotonation from the carboxylic acid-addition complex **6** depending on the reaction sequence of the ligand deprotonation and the carboxylate anion dissociation. The reaction requires additional base, and base was found to play important roles in the generation of the active catalyst **3** from the chloride ruthenium complex **2** and from the stable carboxylic acid-addition complex **6**. Consistent with the experimental results, we predict complex **5** to be the resting state in aqueous solution. However, for convenience we have used complex **3** which is in equilibrium with complex **5** as the active catalyst in our discussions. In agreement with the experimental results, the calculations also predict that the reaction does not produce ester. The chemoselectivity for acid over ester involves two points. First, the formation of carboxylate anion drives the reaction to produce acid and will thus consume any traces of ester produced. Second, the cleavage of water by catalyst **3** in the pathway for producing acid is more favorable than the cleavage of alcohol by catalyst **3** in the pathway for producing ester, because water is in excess.

■ ASSOCIATED CONTENT

Supporting Information

Adjustments for the standard-state concentration; optimized geometries of stationary points involved in energy profiles but not shown in the main text; unfavorable pathways for hydrogen release; unfavorable pathways for the formation of the gem-diol; unfavorable transition-state structures for the dehydrogenation of the gem-diol; results for the formation of the active catalyst **3** from the precursor complex **2** under NaOH in toluene; comparison results for M06, TPSS, and LC-ωPBE functionals; and the total energies and Cartesian coordinates of the structures involved in this study. This material is available free of charge via the Internet at http://pubs.acs.org.

■ AUTHOR INFORMATION

Corresponding Author

mbhall@tamu.edu

Notes

The authors declare no competing financial interest.

■ ACKNOWLEDGMENTS

We acknowledge financial support from the National Science Foundation under CHE-1300787. The authors acknowledge the Texas A&M Supercomputing Facility (http://sc.tamu.edu/) for providing computing resources useful in conducting the research reported in this paper. We thank Professor Milstein for informative discussions about the mechanism.

■ REFERENCES

(1) (a) Tojo, G.; Fernandez, M. *Oxidation of Primary Alcohols to Carboxylic Acids: A Guide to Current Common Practice*; Springer: New York, 2007. (b) Sheldon, R. A. *Chem. Soc. Rev.* **2012**, *41*, 1437.

(2) (a) Sato, K.; Aoki, M.; Noyori, R. *Science* **1998**, *281*, 1646. (b) ten Brink, G.-J.; Arends, I. W. C. E.; Sheldon, R. A. *Science* **2000**, *287*, 1636. (c) Zope, B. N.; Hibbitts, D. D.; Neurock, M.; Davis, R. J. *Science* **2010**, *330*, 74.

(3) (a) Zweifel, T.; Naubron, J.-V.; Grützmacher, H. *Angew. Chem., Int. Ed.* **2009**, *48*, 559. (b) Annen, S.; Zweifel, T.; Ricatto, F.; Grützmacher, H. *ChemCatChem* **2010**, *2*, 1286. (c) Trincado, M.; Grützmacher, H.; Vizza, F.; Bianchini, C. *Chem.—Eur. J.* **2010**, *16*, 2751.

(4) (a) Reid, E. E.; Worthington, H.; Larchar, A. W. J. *Am. Chem. Soc.* **1939**, *61*, 99. (b) Franczyk, T. S.; Moench, W. L. *Process for the preparation of carboxylic acid salts from primary alcohols.* US Patent 6,646,160, 2003.

(5) Balaraman, E.; Khaskin, E.; Leitus, G.; Milstein, D. *Nat. Chem.* **2013**, *5*, 122.

(6) For reviews see: (a) Milstein, D. *Top. Catal.* **2010**, *53*, 915. (b) Gunanathan, C.; Milstein, D. *Acc. Chem. Res.* **2011**, *44*, 588.

(7) (a) Zhang, J.; Leitus, G.; Ben-David, Y.; Milstein, D. J. *Am. Chem. Soc.* **2005**, *127*, 10840. (b) Gunanathan, C.; Ben-David, Y.; Milstein, D. *Science* **2007**, *317*, 790.

(8) Balaraman, E.; Gunanathan, C.; Zhang, J.; Shimon, L. J. W.; Milstein, D. *Nat. Chem.* **2011**, *3*, 609.

(9) Kohl, S. W.; Weiner, L.; Schwartsburd, L.; Konstantinovski, L.; Shimon, L. J. W.; Ben-David, Y.; Iron, M. A.; Milstein, D. *Science* **2009**, *324*, 74.

(10) Iron, M. A.; Ben-Ari, E.; Cohen, R.; Milstein, D. *Dalton Trans.* **2009**, 9433.

(11) Li, J.; Shiota, Y.; Yoshizawa, K. J. *Am. Chem. Soc.* **2009**, *131*, 13584.

(12) Zeng, G.; Guo, Y.; Li, S. *Inorg. Chem.* **2009**, *48*, 10257.

(13) Schwartsburd, L.; Iron, M. A.; Konstantinovski, L.; Diskin-Posner, Y.; Leitus, G.; Shimon, L. J. W.; Milstein, D. *Organometallics* **2010**, *29*, 3817.

(14) Yang, X. Z.; Hall, M. B. J. *Am. Chem. Soc.* **2010**, *132*, 120.

(15) Sandhya, K. S.; Suresh, C. H. *Organometallics* **2011**, *30*, 3888.

(16) (a) Li, H.; Wang, X.; Huang, F.; Lu, G.; Jiang, J.; Wang, Z.-X. *Organometallics* **2011**, *30*, 5233. (b) Li, H.; Wang, X.; Wen, M.; Wang, Z.-X. *Eur. J. Inorg. Chem.* **2012**, 5011. (c) Li, H.; Wen, M.; Wang, Z.-X. *Inorg. Chem.* **2012**, *51*, 5716.
(17) Frisch, M. J.; Trucks, G. W.; Schlegel, H. B.; Scuseria, G. E.; Robb, M. A.; Cheeseman, J. R.; Scalmani, G.; Barone, V.; Mennucci, B.; Petersson, G. A.; Nakatsuji, H.; Caricato, M.; Li, X.; Hratchian, H. P.; Izmaylov, A. F.; Bloino, J.; Zheng, G.; Sonnenberg, J. L.; Hada, M.; Ehara, M.; Toyota, K.; Fukuda, R.; Hasegawa, J.; Ishida, M.; Nakajima, T.; Honda, Y.; Kitao, O.; Nakai, H.; Vreven, T.; Montgomery, J. A., Jr.; Peralta, J. E.; Ogliaro, F.; Bearpark, M.; Heyd, J. J.; Brothers, E.; Kudin, K. N.; Staroverov, V. N.; Kobayashi, R.; Normand, J.; Raghavachari, K.; Rendell, A.; Burant, J. C.; Iyengar, S. S.; Tomasi, J.; Cossi, M.; Rega, N.; Millam, J. M.; Klene, M.; Knox, J. E.; Cross, J. B.; Bakken, V.; Adamo, C.; Jaramillo, J.; Gomperts, R.; Stratmann, R. E.; Yazyev, O.; Austin, A. J.; Cammi, R.; Pomelli, C.; Ochterski, J. W.; Martin, R. L.; Morokuma, K.; Zakrzewski, V. G.; Voth, G. A.; Salvador, P.; Dannenberg, J. J.; Dapprich, S.; Daniels, A. D.; Farkas, O.; Foresman, J. B.; Ortiz, J. V.; Cioslowski, J.; Fox, D. J. *Gaussian 09*, revision B.01; Gaussian, Inc.: Wallingford, CT, 2009.
(18) Chai, J.-D.; Head-Gordon, M. *Phys. Chem. Chem. Phys.* **2008**, *10*, 6615.
(19) (a) Hehre, W. J.; Ditchfie, R.; Pople, J. A. J. *Chem. Phys.* **1972**, *56*, 2257. (b) Francl, M. M.; Pietro, W. J.; Hehre, W. J.; Binkley, J. S.; Gordon, M. S.; Defrees, D. J.; Pople, J. A. J. *Chem. Phys.* **1982**, *77*, 3654.
(20) Andrae, D.; Häussermann, U.; Dolg, M.; Stoll, H.; Preuss, H. *Theor. Chim. Acta* **1990**, *77*, 123.
(21) Clark, T.; Chandrasekhar, J.; Spitznagel, G. W.; Schleyer, P. v. R. J. *Comp. Chem.* **1983**, *4*, 294.
(22) Werner, H.-J. P.; Knowles, J.; Knizia, G.; Manby, F. R.; Schütz, M.; Celani, P.; Korona, T.; Lindh, R.; Mitrushenkov, A.; Rauhut, G.; et al. *MOLPRO, a package of ab initio programs*, version 2010.1; http://www.molpro.net.
(23) Keeffe, J. R.; Gronert, S.; Colvin, M. E.; Tran, N. L. J. *Am. Chem. Soc.* **2003**, *125*, 11730.
(24) Marenich, A. V.; Cramer, C. J.; Truhlar, D. G. J. *Phys. Chem. B* **2009**, *113*, 6378.
(25) Fukui, K. *Acc. Chem. Res.* **1981**, *14*, 363.
(26) (a) Cramer, C. J. *Essentials of Computational Chemistry: Theories and Models*, 2nd ed.; John Wiley & Sons, Ltd: New York, 2004; pp 378−379. (b) Vigara, L.; Ertem, M. Z.; Planas, N.; Bozoglian, F.; Leidel, N.; Dau, H.; Haumann, M.; Gagliardi, L.; Cramer, C. J.; Llobet, A. *Chem. Sci.* **2012**, *3*, 2576.
(27) (a) Webster, C. E.; Pérez, L. M.; Hall, M. B. http://www.chem.tamu.edu/jimp2/index.html (accessed May 2006). (b) Hall, M. B.; Fenske, R. F. *Inorg. Chem.* **1972**, *11*, 768. (c) Bursten, B. E.; Jensen, J. R.; Fenske, R. F. J. *Chem. Phys.* **1978**, *68*, 3320.
(28) Rodríguez-Lugo, R. E.; Trincado, M.; Vogt, M.; Tewes, F.; Santiso-Quinones, G.; Grützmacher, H. *Nat. Chem.* **2013**, *5*, 342.
(29) (a) Dobereiner, G. E.; Crabtree, R. H. *Chem. Rev.* **2010**, *110*, 681. (b) Nova, A.; Balcells, D.; Schley, N. D.; Dobereiner, G. E.; Crabtree, R. H.; Eisenstein, O. *Organometallics* **2010**, *29*, 6548. (c) Watson, A. J. A.; Williams, J. M. J. *Science* **2010**, *329*, 635. (d) Li, H.; Wang, Z.-X. *Chin. Sci. Bull.* **2012**, *55*, 1991.
(30) (a) Curtiss, L. A.; Frurip, D. J.; Blander, M. J. *Chem. Phys.* **1979**, *71*, 2703. (b) Halkier, A.; Koch, H.; Jørgensen, P.; Christiansen, O.; Nielsen, I. M. B.; Helgaker, T. *Theo. Chem. Acc.* **1997**, *97*, 150. (c) Schütz, M.; Brdarski, S.; Widmark, P.-O.; Lindh, R.; Karlström, G. J. *Chem. Phys.* **1997**, *107*, 4597. (d) Klopper, W.; van Duijneveldt-van de Rijdt, J. G. C. M.; van Duijneveldt, F. B. *Phys. Chem. Chem. Phys.* **2000**, *2*, 2227.
(31) Montag, M.; Zhang, J.; Milstein, D. J. *Am. Chem. Soc.* **2012**, *134*, 10325.